

An inverse scattering problem to reconstruct 3D refractive index distributions

UNIVERSITY OF TWENTE.

Narasimhan Kannan

Department of Applied Mathematics
University of Twente

Graduation Committee :

Prof. Stephan van Gils (Applied Analysis Chair)
Dr. Christoph Brune, DAMUT, University of Twente
Prof. Dr. ir. Ivo Vellekoop, BMPI, University of Twente
Dr. ir. Gerrit Meinsma, DAMUT, University of Twente

26 September, 2019

Acknowledgements

I would like to thank to Prof. Stephan van Gils for being supportive since day one. He has always given me the freedom and the encouragement to pursue my interests in mathematics.

I am immensely grateful to Dr. Christoph Brune and Prof. Dr. ir. Ivo Vellekoop for supervising me. Their extreme support, patience and willingness to teach is something I greatly admire. This thesis was only possible under their guidance.

I also want to thank the BMPI group for creating a friendly environment, whose members were always available when you needed help. I also want to thank Daniel Cox (master student in BMPI) for creating the phantom data used in this thesis.

Finally, I would like to thank my friends and family for supporting me throughout my master study.

Abstract

Optical tomography is used for noninvasive imaging of biological samples in microscopy. Light propagation in complex media is a difficult process to analyze and control. A key challenge is to identify a significant parameter which describes the inhomogeneous scattering in tissue, called the refractive index.

In literature it has been shown numerically that one can reconstruct the refractive index distribution via a beam propagation model and convex optimization. Major obstacles for accurate reconstruction are an increasing sample depth and a limited field of view. Hence, it is essential to tackle the ill-posedness and nonlinear dependence in the refractive index estimation.

This thesis introduces regularized variational methods for the non-convex refractive index estimation problem. To achieve accurate reconstructions, state-of-the-art stochastic and non-convex splitting methods are introduced for this problem and compared in realistic numerical simulations.

Contents

1	Introduction	1
1.1	Overview of the problem	2
1.2	Research Goals	4
1.3	Organization	4
2	Model	5
2.1	Forward model	5
2.2	Inverse scattering problem	9
2.3	Problem setup	11
2.4	Tools	12
3	Convex Optimization	17
3.1	Optimality condition	17
3.2	Gradient descent	18
3.3	Stochastic gradient	20
4	Non-convex Optimization	23
4.1	Non-convex approach	23
4.2	Proximal alternating linearized minimization (PALM)	24
4.3	Remarks	28
5	Results and Discussion	29
5.1	Research Goals	29
5.2	Analysis	32
5.2.1	Convergence Behavior	32
5.2.2	Residual Comparison	34
6	Conclusion	39
	Bibliography	41
	Appendix A	43

Chapter 1

Introduction

In microscopy, the main task is to observe, study and control microscopic objects and systems. The type of microscope used to do this depends on the object or the system in question mainly because of its nature. In biomedical applications, for example, low frequency light is used for illumination since it is less scattering. For imaging purposes, the scattering process through the medium needs to be understood in terms of a model if one is interested in reconstructing the scattering object. Further, the propagation of light in scattering medium is itself an interesting topic of study.

The propagation of light can be described by the composition of the medium. A homogeneous medium is a medium with constant density. In the simple setting where a light wave propagates from one homogeneous medium to another with a different refractive index, it experiences a change in its path and in its speed. Figure 1.1¹ gives a geometrical interpretation of the phenomenon. To this end let the speed of light in vacuum be c and the speed in the given medium (with an uniform density distribution) be v_{medium} . The ratio by represented by n , is given by

$$n = \frac{c}{v_{medium}} \quad (1.1)$$

is called the refractive index of the medium with respect to vacuum. Thus, an inhomogeneous medium can be considered to be a distribution of refractive indexes. When light propagates through such a medium the varying distribution of refractive index causes multiple scattering of the light wave. In the latter case when the knowledge of refractive index distribution is absent one can use wavefront shaping to focus light through the medium [1][2]. By focusing light inside the medium one can derive many applications such as imaging, focusing and the propagation of light in inhomogeneous medium is itself interesting in its own right.

¹Image taken from Wikipedia. See Appendix for link.

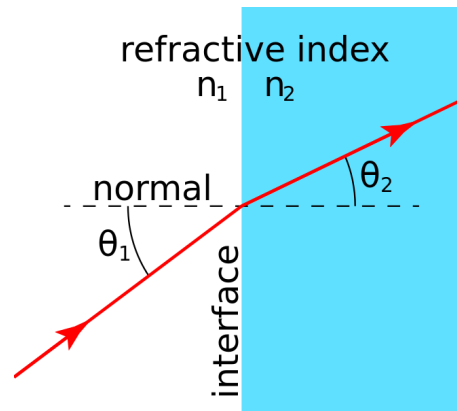


Figure 1.1 Refractive index. As light encounters a new medium with there is change in its and speed given by the relation in Eq.(1.1).

1.1 Overview of the problem

The goal of this study is to reconstruct the refractive index distribution of a given sample by illuminating it with light. We discuss step by step the necessary elements that are required to explain the setup and describe the process of reconstruction.

Tomography

In the field of imaging science, tomography is the process of reconstructing a 3D object by looking at 2D images from various directions. The process of acquiring such 2D images can be done by allowing some wave to penetrate through the object and measuring the response. The reconstruction is done using the response to recover the essential characteristics of the object which cannot be directly identified. For example, in computed tomography, which is widely used in medical applications, the X-ray source and the detector are moved about the object collecting 2D images. Using these 2D images a volumetric image is computed. In our work we use plane waves²(here and after, treated as scalar waves) for illumination. More specifically we use light waves of near-infrared³ wavelength for the illumination. The sample medium, which is illuminated, is assumed to represent an inhomogeneous medium, such as a biological tissue.

Diffraction

In microscopy, since objects are of the order 10^{-6} m, the wave property of light cannot be ignored and we have to take in account the behavior of light at this scale. The bending of a wave around the edge of an obstacle as it passes around it, is called diffraction. Diffraction is exhibited by all waves. Figure

²See Chapter 2 for definition.

³Near-infrared wavelength: 700nm - 2500nm.

1.2⁴ shows the diffraction effect observed when a scalar wave passes through a wavelength-sized slit. It is very interesting to see how the slit acts like a point source for the resulting diffracted wave. Thus, for microscopic objects, when illuminated with light of near-infrared, diffraction effects become prominent.

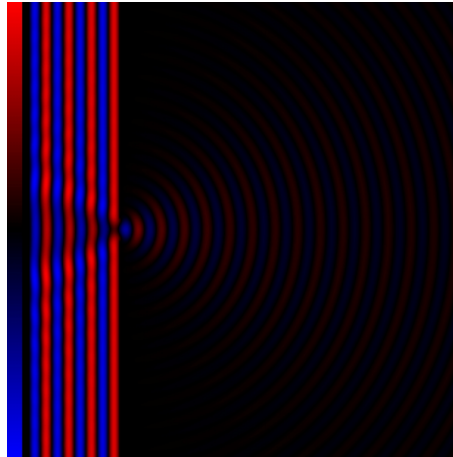


Figure 1.2 Diffraction of a scalar plane wave passing through a small slit.

Motivation

The motivation for approaching the problem of reconstructing refractive index distributions arises mainly for biomedical applications. Here, one usually uses Diffraction tomography with Born or Rytov Approximation, which is based on the Fourier Diffraction Theorem. A detailed treatment can be found in [3]. In this study we take a completely different approach, based on a work recently done in [4].

In [4] the authors use the Beam propagation method (BPM) for simulating propagation of light with a given 3D refractive index distribution. The method lies in the simplicity of the model, where one ignores the absorption and the reflection, considering only the forward propagation. Further, one can split the propagation step of the input wave field and perform an equivalent backpropagation step (the adjoint) to the output wave field. The details of the front propagation and back propagation are described in Chapter 2.

In our work we aim to improve upon the method, particularly involving the optimization methods. In [4] the authors assume that the objective function that is being optimized is convex in the refractive index. We drop this assumption and apply a recently developed non-convex optimization method [5] to optical phase tomography (using BPM) for the first time.

⁴Image taken from Wikipedia. https://commons.wikimedia.org/wiki/File:One_wave_slit_diffraction_dirichlet_bw.gif.

1.2 Research Goals

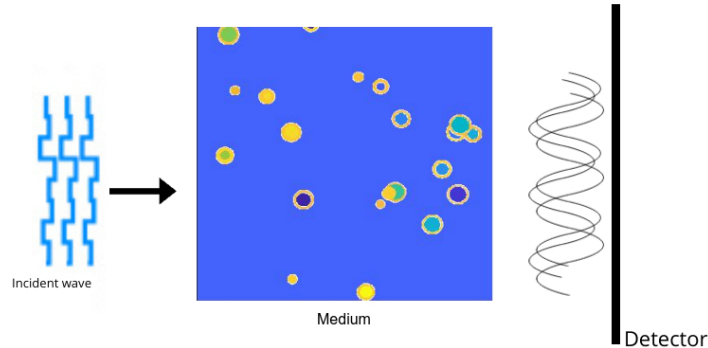


Figure 1.3 Setup showing light wave propagating through a medium containing small beads having different refractive index.

From the given wave propagation of light, we use convex and non-convex optimization methods to compare the reconstruction accuracy. It is expected that the non-convex optimization methods are better than the convex techniques, in the sense of accurate structural reconstruction. Further, we want to answer the following research questions;

1. : What is the relation between thickness of the sample and the quality of reconstruction?
2. : Which optimization model shows promise for the best reconstruction?

1.3 Organization

The organization of the document is as follows; in Chapter 2 we discuss the necessary theory, properties of the model and derive tools which will be used later in the chapters. In Chapter 3 we discuss convex optimization methods, namely Gradient descent and Stochastic Gradient descent. Next, in Chapter 4 we see non-convex optimization methods and note down important definitions and concepts which will be required. In Chapter 5 we compare the results of all the optimization methods and discuss their behavior. Finally, we conclude by an outlook on the results and what can be done in the future.

In the Appendix one can find definitions of convex, Fourier transform and subdifferential, which are used.

Chapter 2

Model

To approach the problem reconstructing the refractive index we need a model. The model should have explicit dependence on the refractive index. Further, we also want the model to produce the correct output given an input. In the theory of inverse problems, there are two major classifications; forward problem and inverse problem. The forward problem consists of determining the mapping which gives the correct output. The inverse problem consists of determining the causal factors of a given output.

To begin with, we look at the forward model, the Beam Propagation Method (BPM). Then, we move to the Inverse problem and derive necessary tools used in later chapters. Finally, we discuss the problem setup and an overlook of the reconstruction procedure.

2.1 Forward model

Given a process which is defined by a specific set of parameters and takes in some input, which is assumed to be in the user's control, the problem of getting the desired output from this process is called the *forward problem*, see figure 2.1. In the context of this work, the process here is light propagation through complex media. Therefore, if we can find a model which describes the propagation of light through any medium then we have solved the forward problem.

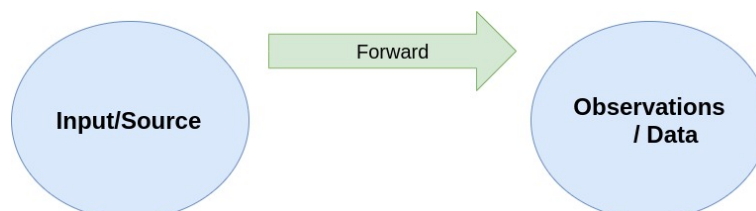


Figure 2.1 Forward Problem

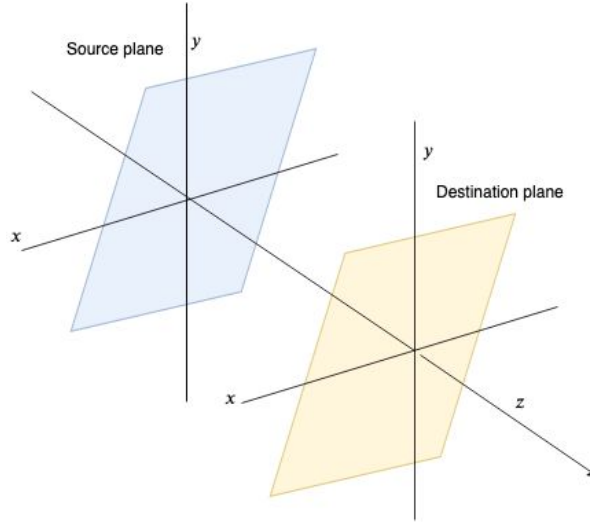


Figure 2.2 Angular Spectrum Method

Now suppose we want to model the propagation of light through an inhomogeneous medium which is described a refractive index distribution in space. For this we need to calculate how the light behaves at each of these points in space. This is accomplished by BPM which uses the angular spectrum method (ASM). Given any plane wave field (scalar), ASM allows one to propagate it through a homogeneous medium.

Angular Spectrum Method

Planes waves can be thought of as the field generated by a point source located at infinity. Thus, field points in the plane perpendicular to the direction of propagation will correspond to the same phase. Hence, one can denote a plane wave as,

$$E_{plane} = e^{i(k \cdot r)}$$

Here, k is the wave vector and r is the position vector. The wave vector is related to the wave number by, $k_x^2 + k_y^2 + k_z^2 = k_0^2$ and $k_0 = \frac{2\pi}{\lambda}$.

The Angular spectrum method by which one can propagate a plane wave through a homogeneous medium (described below). The process can be mathematically written as follows:

1. Given E_{in} , Fourier transform it,

$$\tilde{E}_{in} = \mathcal{F}E_{in} \quad (2.1)$$

$$\tilde{E}_{in}(k_x, k_y, z_0) = \iint E_{in}(x, y, z_0) e^{ik_x x + ik_y y} dx dy \quad (2.2)$$

where \mathcal{F} is the 2D Fourier transform.

2. Propagate in the z direction by z_1 amount,

$$\tilde{E}(k_x, k_y, z_1) = e^{ik_z z_1} \tilde{E}_{in}(k_x, k_y, z_0) \quad (2.3)$$

k_z is computed through the relation $k_z = \sqrt{k_0^2 n_{avg}^2 - k_x^2 - k_y^2}$. Here, n_{avg} is the average refractive index of that phase screen.

3. Apply inverse Fourier transform,

$$E(x, y, z_1) = \mathcal{F}^{-1} \tilde{E}(k_x, k_y, z_1) \quad (2.4)$$

From here on we will denote the above steps by \mathcal{P} .

Beam Propagation Method

When the waves enter the complex media they experience scattering. These scattered waves become more disordered as we go deeper in the medium. To model this scattering we can represent these particles by their refractive index. Since the media is continuous and disordered, to apply ASM we discretize the media into a finite number of thin slices representing the distribution of refractive index in that plane. To represent the scattering process in a single slice of thickness dz , we first propagate half way ($\frac{dz}{2}$), apply scattering and the propagate the rest of the half distance $\frac{dz}{2}$. The process can be represented as follows,

1. Propagate half way by a distance $\frac{dz}{2}$,

$$E(x, y, z_0 + dz/2) = \mathcal{P}_{\frac{1}{2}} E_{in}(x, y, z_0)$$

where $\mathcal{P}_{\frac{1}{2}}$ denotes the half way propagation.

2. Apply scattering, $e^{i\varphi(x,y)}$,

$$E_{scat}(x, y, z_0 + dz/2) = e^{i\varphi(x,y)} E(x, y, z_0 + dz/2) \quad (2.5)$$

where $\varphi(x, y) = k_0 dz (n_{avg} - n(x, y))$. Here, n_{avg} is the average refractive index of that slice and $n(x, y)$ is the refractive index distribution for that slice.

3. Propagate remaining half way,

$$E_{out}(x, y, z_1) = \mathcal{P}_{\frac{1}{2}} E_{scat}(x, y, z_0 + dz/2)$$

Therefore, by assuming paraxial approximation (neglecting the reflected field) one can think of a complex media being composed of M number of slices. Denoting each of the scattering processes

described above by \mathcal{B}_m , where the index m denotes the m^{th} -slice, we have,

$$\mathcal{B}_m(\cdot) = \mathcal{P}_{\frac{1}{2}} e^{i\varphi_m} \mathcal{P}_{\frac{1}{2}}(\cdot) \quad (2.6)$$

We can assume that each of these M slices are of thickness dz , then the above process can be repeated M times. Thus, the propagation through this media can be written as the following composition,

$$\mathcal{T}(n; \cdot) := \mathcal{B}_M \cdot \dots \mathcal{B}_m \cdot \dots \mathcal{B}_1 \quad (2.7)$$

$$E_{out} = \mathcal{T}(n; E_{in}) \quad (2.8)$$

Here, E_{out} denotes the model's output field.

It is important to note all the assumptions that have been made about the model and see the limitations which follow. This will enable us to carefully model the inverse problem.

Assumptions:

1. Paraxial approximation: The BPM model is obtained by assuming paraxial approximation when solving the Helmholtz equation. A detailed derivation of the BPM model is given in [6]. To simulate the propagation of a wave through a media exactly (analytically) one uses the Born or the Rytov approximation.
2. Another effect that is neglected is absorption by the media. In the case of biological tissues the absorbed light maybe released as vibrations.
3. The refractive index values should not change abruptly in consecutive slices.

Consequences:

1. Assumption 1 implies we ignore the reflections and consider only the forward propagation.
2. Assumption 2 tells us there is no absorption, hence there is only scattering. This makes the model unitary, that is, $\mathcal{T}\mathcal{T}^\dagger = \mathcal{T}^\dagger\mathcal{T} = \mathbb{I}$.
3. Assumption 3 implies the number of slices due to discretization has a lower limit. A detailed analysis on this can be found in [6].

Now, the important properties of the BPM model will be listed out.. Here the model is denoted by $\mathcal{T}(n; E)$.

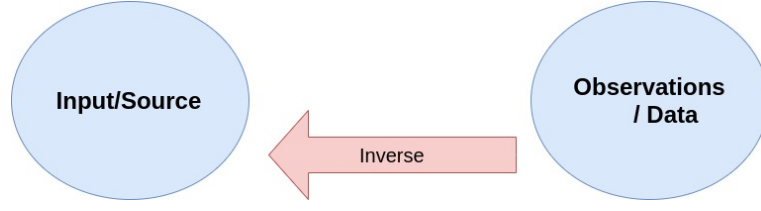


Figure 2.3 Inverse Problem

Properties:

1. $\mathcal{T}(n; E)$ is linear in E for fixed n .
2. For a fixed E $\mathcal{T}(n; E)$ is non linear in n
3. The consequence 2, that is by neglecting the absorption factor, $\mathcal{T}(n; \cdot)$ becomes unitary. This can be seen in the description given in Eq.(2.7).

Before we proceed further lets summarize the effect of change in the refractive index when a plane wave propagates through it. Eq.(2.5) tells us that each voxel of refractive index causes a phase delay in the plane wave's phase. Thus, given a plane wave and a 3D refractive index distribution, as the plane wave propagates through this distribution it undergoes a series of phase delays.

2.2 Inverse scattering problem

Inverse problems can be categorized into two classes of problems; inverse source problem(ISP) and the inverse scattering problem. In the first one, ISP, when one is given the observations and the model, the problem is to find the source, which is the causal factor of the observations. While in the inverse scattering problem one deals with problem of finding the parameters that describe the model.

In the problem of reconstructing refractive index distributions, one usually uses diffraction tomography, which involves solving the Helmholtz equation using Born or the Rytov approximation. But it has been shown in [4], that using the BPM and error reduction method one can reconstruct refractive index distributions. Thus, our inverse scattering problem is to use BPM and reconstruct the refractive index distribution from observed complex field values.

The simplest way to approach is by minimizing the error between the measured field and the computed field from the model. Thus, we aim to minimize the following over the refractive index distribution,

$$\min_n \{ \mathcal{E} := \frac{1}{J} \sum_{j=1}^J \| \mathcal{T}(n; E_{in.j}) - E_{meas.j} \|_2^2 \} \quad (2.9)$$

where $\mathcal{T}(n; E_{in})$ is the model's output, E_{meas} is the measured field. The term in Eq.(2.11) is called the data fidelity term. Therefore, the goal of the inverse scattering problem is to reconstruct the \mathcal{T} map from the field measurements.

Ill-posedness

In the study and the application of inverse problems, the concept of regularization plays a major role. It allows one to use the prior knowledge about the problem, such as constraints on the problem which do not explicitly occur in the data fidelity. Before we discuss regularization we first look at the *ill-posedness* of a problem. A problem is said to be *well-posed* if it satisfies the following three conditions;

The problem

1. has a solution (Existence)
2. has a unique solution (Uniqueness)
3. has a small change in the solution when there is a small change in the initial condition (Stability)

Thus, a problem is said to be *ill-posed* if it fails to satisfy any one of the above following criteria. In practice most inverse problems are ill-posed. One can also define the degree of ill-posedness of a given problem and make appropriate assumptions for the reconstruction. A good introduction and detail can be found in the work, [7]. We will not discuss the degree of ill-posedness of the BPM model.

Clearly, our problem is ill-posed. First, propagation of light is described by the Helmholtz equation and since the BPM model is an approximation, an unique solution does not exist. That is, one can make a small change in the refractive index and still get the same outcome. Next, in tomography one usually faces the problem of field of view. Here, one is limited by the amount of measurements one can make. For example, in microscopy, for a noninvasive procedure one can only make observations from the surface. Thus, for a perfect reconstruction one would ideally require a complete set of observations from all the possible angles.

Regularization

The cause of ill-posedness can be due to many reasons such as; restriction in measurement parameters, availability of limited data, noise, etc. To tackle the general problem of reconstruction one uses some known information about the system, which is not explicitly present in the reconstruction process, and tries to optimize along the main reconstruction problem, see Eq.(2.11). This additional term which is added to the data fidelity is called the *Regularization* term and the coefficient of it is called the regularization parameter.

In our study we only use the total variation regularizer, since the phantoms we simulate have smooth edges.

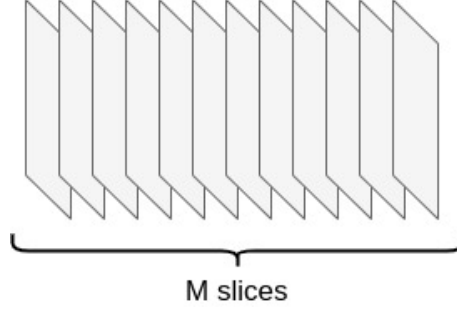


Figure 2.4 Discretization of sample into M slices.

Total Variation (TV)

The main idea of applying a total variation regularizer is to resolve the sharp boundaries. If one has the knowledge that the original system has objects with sharp boundaries (assuming that the reconstruction is done for imaging), then it makes sense to minimize the total variation in the image (reconstruction). Mathematically,

$$\mathcal{R}(n) = \int |\nabla n| \quad (2.10)$$

In this work, we will use an approximation of the gradient of TV since it is not well-defined.

With the above the addition the problem to be optimized becomes,

$$\min_n \{ \mathcal{E} := \frac{1}{J} \sum_{j=1}^J \|\mathcal{T}(n; E_{in,j}) - E_{meas,j}\|_2^2 + \alpha \mathcal{R}(n) \} \quad (2.11)$$

2.3 Problem setup

To realize this problem we describe the setup of acquiring the output leaving out the experimental details. That is, all the components of the process which have mathematical significance for the optimization procedures. In similar scenarios where the analysis can be done without the explicit need for the instruments and devices, the methods are called *device-independent methods*.

Here we describe the how we assign the refractive index in the slices, a collection of these slices represent a physical sample with the refractive index distribution of a given thickness, see Figure 2.4. In Figure 2.5 $\Delta n(x, y, z)$ denotes the difference between the refractive index at the position and the background. In the BPM model, this is calculated as the difference between the refractive index at that position and the average of the whole slice. Therefore, by continuing this for all the slices we have a refractive index distribution. Figure 2.6 shows the schematic of the whole optimization process.

The parameters that we have control on are :

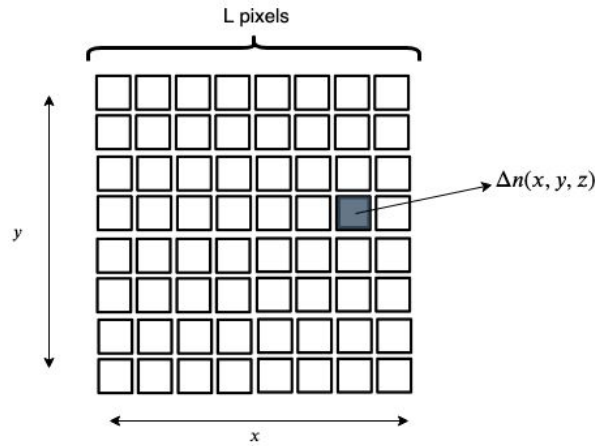


Figure 2.5 Figure showing the realization of refractive index distribution in the BPM model.

1. Input plane wave
2. Beam propagation method, here the input plane wave can be propagated forward through a specified refractive index map. One can backpropagate the wave, which is mathematically the adjoint of the forward operation.
3. Refractive index distribution of the object which is updated at iteration step of the optimization procedure.

2.4 Tools

Dependence on n

The BPM model explicitly depends on the refractive index distribution. In our study we use gradient based methods, so it will be useful to calculate the gradient of the fidelity which will be used in the later chapters. To begin with, let the media be discretized in to M number of slices with each slices containing $L \times L$ entries (2D array), see Figure 2.4 and fig:rimap. Expressing it in the vector form, we have, $n_m = (n_{m,1} \dots n_{m,L \times L})$ we can write,

$$\frac{\partial \mathcal{E}_1}{\partial n_m} = \begin{bmatrix} \frac{\partial \mathcal{E}_1}{\partial n_{m,1}} \\ \cdot \\ \cdot \\ \frac{\partial \mathcal{E}_1}{\partial n_{m,l}} \\ \cdot \\ \cdot \\ \frac{\partial \mathcal{E}_1}{\partial n_{m,L \times L}} \end{bmatrix} \quad (2.12)$$

The above entries, where $m \in \{M\}$ and $l \in \{L \times L\}$, are given by,

$$\frac{\partial \mathcal{E}_1}{\partial n_{m,l}} = \frac{1}{J} \sum_j^J \left[\frac{\partial E_{out,j}^\dagger}{\partial n_{m,l}} (E_{out,j} - E_{meas,j}) + (\bar{E}_{out,j} - \bar{E}_{meas,j}) \frac{\partial E_{out,j}}{\partial n_{m,l}} \right] \quad (2.13)$$

$$= \frac{1}{J} \sum_j^J \left[2 \operatorname{Re} \left\{ (\bar{E}_{out,j} - \bar{E}_{meas,j}) \frac{\partial E_{out,j}}{\partial n_{m,l}} \right\} \right] \quad (2.14)$$

Re denotes the real part, $\bar{\cdot}$ denotes complex conjugate.

Recall that $E_{out,j}$ is the j^{th} output of the BPM and $E_{meas,j}$ is the j^{th} measured field. Then the differential of the output field of the BPM w.r.t the l^{th} component of the j^{th} observation, i.e. $\frac{\partial E_{out,j}}{\partial n_{m,l}}$ is

$$\frac{\partial E_{out,j}}{\partial n_{m,l}} = \frac{\partial}{\partial n_{m,l}} (\mathcal{A}_k \mathcal{P}_{\frac{1}{2}} e^{i\varphi_m} \mathcal{P}_{\frac{1}{2}} \mathcal{C}_{m-1} E_{in,j}) \quad (2.15)$$

$$= \mathcal{A}_m \mathcal{P}_{\frac{1}{2}} \left(\frac{\partial e^{i\varphi_m}}{\partial n_{m,l}} \right) \mathcal{P}_{\frac{1}{2}} \mathcal{C}_{m-1} E_{in,j} \quad (2.16)$$

$$= \mathcal{A}_m \mathcal{P}_{\frac{1}{2}} (i e^{i\varphi_m^l}) \mathcal{P}_{\frac{1}{2}} \mathcal{C}_{m-1} E_{in,j} \quad (2.17)$$

where c is a constant, which is ignored from here on, and with

$$\mathcal{A}_m = \prod_m^M \mathcal{B}_m$$

$$\mathcal{C}_m = \prod_1^m \mathcal{B}_m$$

where \mathcal{B}_m is defined as earlier in Eq.(2.6).

Now following from Eq.(2.14), the l^{th} component is given by,

$$\frac{\partial \mathcal{E}_1}{\partial n_{m,l}} = \frac{1}{J} \sum_j^J \left[2 \operatorname{Re} \left\{ (\bar{E}_{out,j} - \bar{E}_{meas,j}) \mathcal{A}_m \mathcal{P}_{\frac{1}{2}} (i e^{i\varphi_m^l}) \mathcal{P}_{\frac{1}{2}} \mathcal{C}_{m-1} E_{in,j} \right\} \right] \quad (2.18)$$

The term in the real part above can be written in the inner product form as

$$\begin{aligned} (\bar{E}_{out,j} - \bar{E}_{meas,j}) \mathcal{A}_m \mathcal{P}_{\frac{1}{2}} (i e^{i\varphi_m^l}) \mathcal{P}_{\frac{1}{2}} \mathcal{C}_{m-1} E_{in,j} &= \langle \mathcal{A}_m \mathcal{P}_{\frac{1}{2}} (i e^{i\varphi_m^l}) \mathcal{P}_{\frac{1}{2}} \mathcal{C}_{m-1} E_{in,j}, E_{out,j} - E_{meas,j} \rangle \\ &= \langle \mathcal{A}_m \mathcal{P}_{\frac{1}{2}} (i e^{i\varphi_m^l}) \mathcal{P}_{\frac{1}{2}} \mathcal{C}_{m-1} E_{in,j}, \mathcal{A}_m \mathcal{C}_{m-1} E_{in,j} - (\mathcal{A}_m \mathcal{A}_m^\dagger) E_{meas,j} \rangle \\ &= \langle \mathcal{P}_{\frac{1}{2}} (i e^{i\varphi_m^l}) \mathcal{P}_{\frac{1}{2}} \mathcal{C}_{m-1} E_{in,j}, \mathcal{C}_{m-1} E_{in,j} - (\mathcal{A}_m^\dagger) E_{meas,j} \rangle \end{aligned} \quad (2.19)$$

Thus, Eq.(2.18) becomes,

$$\frac{\partial \mathcal{E}}{\partial n_{m,l}} = \frac{1}{J} \sum_j^J [2 \operatorname{Re} \{ \langle \mathcal{P}_{\frac{1}{2}}(ie^{i\phi_m^l})\mathcal{P}_{\frac{1}{2}}\mathcal{C}_{m-1}E_{in,j}, \mathcal{C}_{m-1}E_{in,j} - (\mathcal{A}_m^\dagger)E_{meas,j} \rangle \}] \quad (2.20)$$

The above term should be equal to zero for all $m \in \{M\}$ and $l \in \{L \times\}$ for optimality. Here, \mathcal{A}_m^\dagger is the Hermitian adjoint of the forward propagation, which represents the backpropagation part of the model.

TV approximation

The TV regularizer is not differentiable a function. Further, for the BPM model it is not possible to derive a primal-dual formulation, hence we need to use an approximation of the TV regularizer. We can do the approximation by adding a small positive number, $\varepsilon > 0$ to the TV term.

$$\mathcal{R}_\varepsilon(n) = \int \sqrt{|\nabla n|^2 + \varepsilon}$$

To calculate the gradient, we treat each slice as a 2D image, then use the in-built MATLAB function *imgradient*¹. The differential of the TV approximation is then given by,

$$\frac{\partial \mathcal{R}_\varepsilon(n)}{\partial n} = \nabla \cdot \frac{\nabla n}{|\nabla n| + \varepsilon}$$

¹<https://nl.mathworks.com/help/images/ref/imgradient.html>

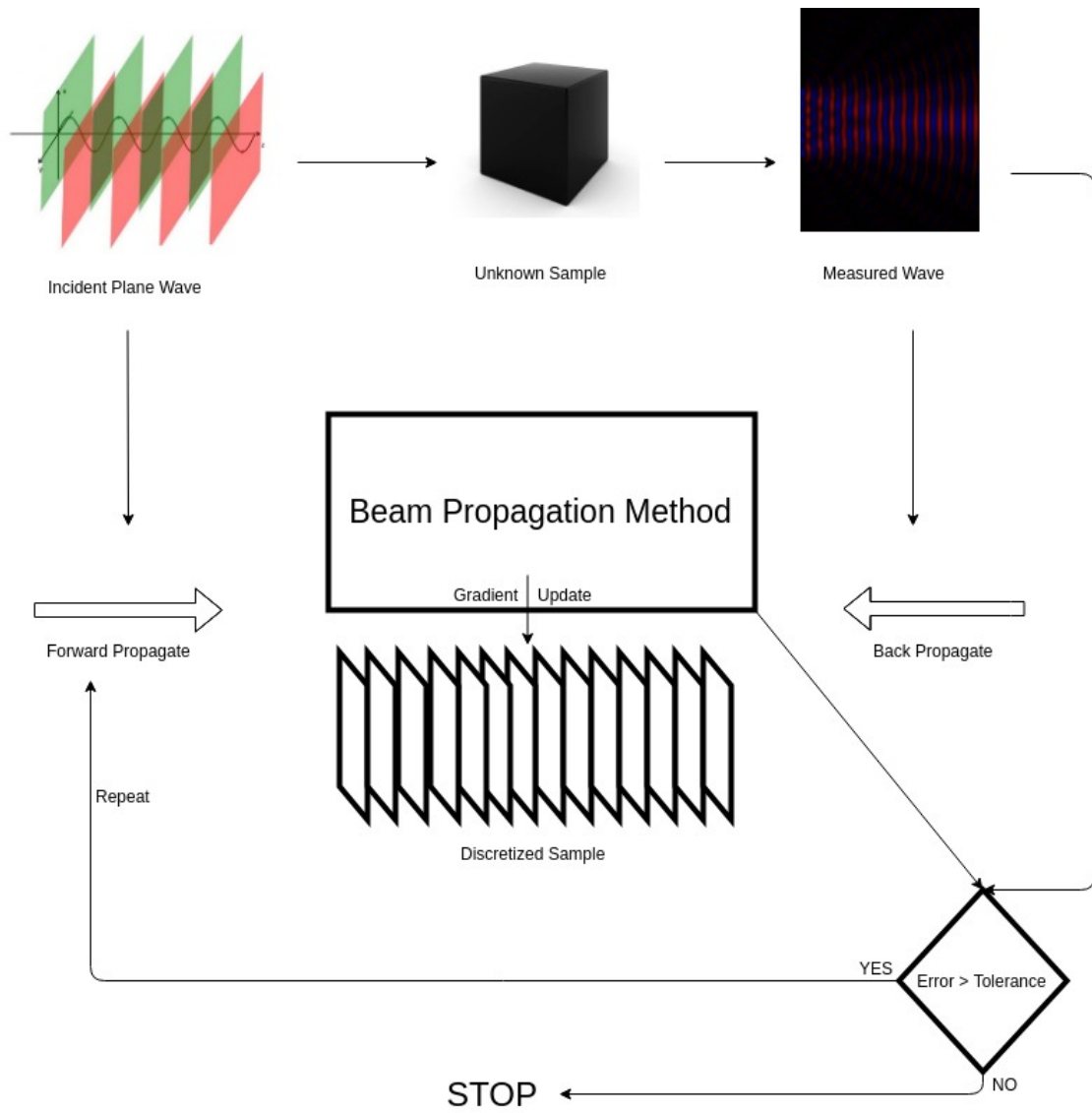


Figure 2.6 Schematic for reconstructing the refractive index distribution using BPM.

Chapter 3

Convex Optimization

The most common optimization approaches are done in the convex setting. This is primarily because the convexity of a continuous (at least piecewise) functions guarantees the convergence to an optimal solution. In this chapter we first assume that the given objective function is convex, this is called convex relaxation. Next, we use the gradient derived in Chapter 2 to perform iterative gradient based algorithm. We are well aware, that the problem of reconstructing the refractive index distributions is a non-convex problem. Nevertheless, it is quite possible we get a solution which gives out a distribution of the refractive index with some structural information. To begin with, motivated by [4], we perform standard Gradient descent approach.

In this chapter we provide necessary elements for implementing convex optimization techniques, namely Gradient Descent (GD) and Stochastic Gradient Descent (SDG). We start with the optimality conditions required for the GD method. Then we formally state the GD method and the algorithm. Next, we follow a similar procedure for SGD.

3.1 Optimality condition

By assuming the convex relaxation of the problem, Eq.(2.11), we use the following Lemma to arrive at the optimality condition for applying gradient based methods.

Lemma 1 (Optimality Condition) *Let $f : \mathbb{R} \rightarrow \mathbb{R}$ be a convex and differentiable function. Let $\Omega \subset \mathbb{R}^d$ be convex. Then x is an optimal solution for the convex problem,*

$$\min f(x) \quad \text{such that } x \in \Omega$$

if and only if $x \in \Omega$ and

$$\nabla f(x)^T (y - x) \geq 0 \quad , \forall y \in \Omega$$

Therefore, for $x \in \Omega$ and is an optimal solution, then we must have $\nabla f(x) = 0$. Then the condition for optimality can be derived by setting the gradient of the objective, Eq.(2.11), w.r.t the refractive index to zero.

$$\frac{\partial \mathcal{E}(n)}{\partial n} = 0$$

To this end, as per the model, the discretization of the medium is done such that each of the slice is further discretized into a 2D array representing the refractive index distribution of that slice. Thus, the gradient for that entry is given by the following steps:

3.2 Gradient descent

We want minimize the objective function eq.(2.11),

$$\min_{n \geq 1} \{ \mathcal{E}(n) := \frac{1}{J} \sum_j \|\mathcal{T}(n)E_{in,j} - E_{meas,j}\|^2 + \alpha \mathcal{R}_\epsilon(n) \} \quad (3.1)$$

where $\mathcal{R}(n)$ is the regularization term.

With the optimality condition, the gradient descent for the p^{th} iteration can be formulated as follows,

$$n_{p+1} = n_p - \gamma \frac{\partial \mathcal{E}}{\partial n_p} \quad (3.2)$$

where γ is a constant and denotes the step-size.

Assuming that the gradient approaches zero, it is also necessary that the step sizes are optimal. This can be controlled by choosing the step-size. One way to choose the step-size at every iteration is by calculating the Lipschitz constant of the gradient.

Definition 3.2.1 (Lipschitz continuity) *Let X, Y be two real vector spaces. A function $f : X \rightarrow Y$ is called Lipschitz continuous if there exists a constant $K > 0$ such that the following holds,*

$$\|f(x_1) - f(x_2)\| \leq K \|x_1 - x_2\| \quad \forall x_1, x_2 \in X$$

K is called the Lipschitz constant.

Theorem 1 *Let $f : \mathbb{R}^d \rightarrow \mathbb{R}$ a convex and differentiable function with its gradient being Lipschitz continuous, $K > 0$. Then if we run the gradient descent for p iterations with a fixed step size γ such that $\gamma \leq \frac{1}{K}$, it will converge to a solution $f^{(p)}$ satisfying,*

$$f(x^{(p)}) - f(x^*) \leq \frac{\|x^{(0)} - x^*\|_2^2}{2\gamma p}$$

where $f(x^*)$ is the optimal solution.

Proof: For proof one can see [8].

From the above definition and the explicit expression of the gradient we can calculate the Lipschitz constant of the gradient as follows:

The gradient is taken with respect to each (scalar) $n1_{m,l}$ and $n2_{m,l}$. For the sake of simplicity lets denote them as n_1 and n_2 . So for a fixed j^{th} single plane wave and from eq.(??) we have,

$$\left\| \frac{\partial \mathcal{E}_1}{\partial n_1} - \frac{\partial \mathcal{E}_1}{\partial n_2} \right\| = \left\| \text{Re} \left\{ \langle P_{\frac{1}{2}} (i(e^{i\varphi_1} - e^{i\varphi_2}) P_{\frac{1}{2}} \mathcal{C}_{m-1} E_{in,j}, (\mathcal{C}_{m-1} E_{in,j} - (\mathcal{A}_m^\dagger) E_{meas,j}) \rangle \right\} \right\| \quad (3.3)$$

where $\varphi_1 = k_0 dz(n_{1avg} - n_1)$ and $\varphi_2 = k_0 dz(n_{2avg} - n_2)$. Note that the inner product is taken w.r.t each of the component (m, l) , so the exponentials can be treated as scalars for each of the inner product.

$$\left\| \frac{\partial \mathcal{E}_1}{\partial n_1} - \frac{\partial \mathcal{E}_1}{\partial n_2} \right\| = \left\| \text{Re} \left\{ (i(e^{i\varphi_1} - e^{i\varphi_2}) \langle P_{\frac{1}{2}} \mathcal{C}_{m-1} E_{in,j}, P_{\frac{1}{2}}^\dagger (\mathcal{C}_{m-1} E_{in,j} - (\mathcal{A}_m^\dagger) E_{meas,j}) \rangle \right\} \right\| \quad (3.4)$$

Now to simplify calculations further denote,

$$\begin{aligned} \mathcal{C}_{m-1} E_{in,j} &= z_{m-1} \\ P_{\frac{1}{2}} \mathcal{C}_{m-1} E_{in,j} &= z_{m-\frac{1}{2}} \\ P_{\frac{1}{2}}^\dagger (\mathcal{A}_m^\dagger) E_{meas,j} &= w_{m+\frac{1}{2}} \end{aligned}$$

$$\left\| \frac{\partial \mathcal{E}_1}{\partial n_1} - \frac{\partial \mathcal{E}_1}{\partial n_2} \right\| = \left\| \text{Re} \left\{ i(e^{i\varphi_1} - e^{i\varphi_2}) [|z_{m-1}|^2 - \langle z_{m-\frac{1}{2}}, w_{m+\frac{1}{2}} \rangle] \right\} \right\| \quad (3.5)$$

$$\leq K \cdot |\varphi_1 - \varphi_2| \quad (3.6)$$

where $K = \left| \text{Re} \left\{ \langle z_{m-\frac{1}{2}}, w_{m+\frac{1}{2}} \rangle \right\} \right| + \left| \text{Im} \left\{ \langle z_{m-\frac{1}{2}}, w_{m+\frac{1}{2}} \rangle \right\} \right| + |z_{m-1}|^2$ is calculated for each gradient step. The above can be proved simple but tedious inequalities involving complex numbers. Thus, if one chooses a step size such that $\gamma_p = \min\{1, \frac{\beta}{K}\}$, where β is a constant, then the convergence to a critical point is optimal.

The Gradient descent can be written in the pseudocode as follows:

Algorithm 1 GD

```

1: procedure GRADIENT DESCENT
2:   Initialize  $n = n_0$ , tolerancelevel = tol
3:   while error > tol do
4:     for j=1 : J do
5:       Choose  $\gamma_j = \min\{\frac{1}{K}, 1\}$ 
6:       Calculate  $\gamma_j \frac{\partial \mathcal{E}(n; E_j)}{\partial n}$ 
7:       Update  $n = n - \frac{1}{J} \sum_{j=1}^J \gamma_j \frac{\partial \mathcal{E}(n; E_j)}{\partial n}$ 
8:       Calculate Error between measured and computed field.
9:   return n and error

```

where K is the Lipschitz constant calculated for each of the observation.

3.3 Stochastic gradient

The stochastic gradient method can be viewed as an approximation to the standard gradient descent method. The basic idea is to randomly choose the gradient of different observations (called batches) and perform the gradient descent method. This is done in the view that the total gradient of all observations contains redundancies and by choosing small subset of those one can approximate the gradient. Suppose we choose a batch of size $|G|$ from J observations the minimization problem becomes,

$$\min_{n \geq 1} \{ \mathcal{E}_2(n) := \frac{1}{G} \sum_{j=1}^G \|\mathcal{J}(n)E_{in.j} - E_{meas.j}\|^2 + \alpha \mathcal{R}_\varepsilon(n) \} \quad (3.7)$$

Then the update is given by

$$n_{p+1} = n_p - \gamma \frac{\partial \mathcal{E}_2}{\partial n_p} \quad (3.8)$$

This procedure, although similar, has a different convergence behavior than the standard gradient descent. Further, in terms of converging speed to the optimal solution, we will see how it affects the convergence.

Similar to the previous section we adopt the Lipschitz constant for the adaptive step size.

Algorithm 2 SGD

```
1: procedure STOCHASTIC GRADIENT DESCENT
2:   Initialize  $n = n_0$ , tolerancelevel = tol
3:   while error > tol do
4:     Randomly choose  $G \subset J$ 
5:     for j=1 : G do
6:       Choose  $\gamma_j = \min\{\frac{1}{K}, 1\}$ 
7:       Calculate  $\gamma_j \frac{\partial \mathcal{E}(n; E_j)}{\partial n}$ 
8:     Update  $n = n - \frac{1}{G} \sum_{j=1}^G \gamma_j \frac{\partial \mathcal{E}(n; E_j)}{\partial n}$ 
9:     Calculate Error between measured and computed field.
10:  return  $n$  and error
```

Chapter 4

Non-convex Optimization

Most application based problems where optimization techniques are used assume convexity at some level. This leads the optimization problem to get stuck in a local minima. There are however methods to avoid getting stuck in local minima, such as the Heavy-ball method [9]. But, even there methods do not guarantee convergence to the optimal solution.

Before we proceed further it is important to note the nature of non-convexity which is used to design the optimization techniques for a given problem. The nature of non-convexity of a problem can be explicit or implicit. More specifically, it would be a good step if one can identify the variables responsible for the non-convex behavior. Then one can split up the problem in those variables and solve the problem. In the case that the nature of non-convexity is implicit, one is aware of the non-convexity of the problem but finds it difficult to identify similar variables responsible for the non-convexity. Then, one requires a different approach to such problems. Recently there have been developments in the methods for optimization of non-convex and nonsmooth functions [5].

Organization: We will first note the basic and the most important definition used in formulating the PALM technique [5], the *proximal* mapping. Then, we go on to an important property which covers the class of those non-convex-nonsmooth functions over which the PALM technique can be applied so as to get an optimal solution. This is namely the KL property. Moving on, we state the PALM algorithm and note the minimal assumptions satisfied by the objective function.

4.1 Non-convex approach

We first begin with addressing the explicit non-convexity part. From the model it is clear that the relationship between the model and the refractive index is nonlinear and its dependence is non-convex.

We address our original problem by stating it in a different way, that is,

$$\min_{n^{(l)} \geq 1} \{ \dots \min_{n^{(1)} \geq 1} \{ \tau \left\| \mathcal{T}(n^{(\cdot)}, E_{in,j}) - E_{meas,j} \right\|^2 + \alpha \mathcal{R}_\epsilon(n) \} \dots \} \quad (4.1)$$

It is very important to notice the difference between Eq.(4.1) and Eq.(3.1). In the latter one, which is the standard gradient descent over all the observations, the update for the new refractive index in the iterative procedure is the average of all the gradients. While in Eq.(4.1), we are trying to solve the minimization problem for each observation. That is, we solve a sequence of optimization problem where each optimization problem depends on the previous update.

Writing down the pseudocode

Algorithm 3 NC

- 1: **procedure** NON-CONVEX APPROACH
 - 2: Initialize $n = n_0$, tolerancelevel = tol
 - 3: **while** error > tol **do**
 - 4: **for** j=1 : J **do**
 - 5: **for** m=1 : M **do**
 - 6: Choose $\gamma_j = \min\{\frac{1}{K}, 1\}$
 - 7: Calculate $\gamma_j \frac{\partial \mathcal{E}(n; E_j)}{\partial n_m}$
 - 8: Update $n = n - \gamma_j \frac{\partial \mathcal{E}(n; E_j)}{\partial n_m}$
 - 9: Calculate Error between measured and computed field.
 - 10: **return** n and error
-

4.2 Proximal alternating linearized minimization (PALM)

In order to apply PALM we need to identify a auxiliary variable, other than the refractive index, which can be used to minimize the objective function. First we make the observation from the convex method that for each slice the gradient of the objective is dependent on the complex field which has propagated through the previous layers. Therefore, for a correct update of the refractive index one has an implicit assumption that the above mentioned complex field is correct. The argument for the correction of the complex field thus applies to all the slices. The motivation for this comes from an approach used in [10]. In [10], the authors use a method similar to BPM, called multislice approach [11], to model the propagation of light. Thus, they make use of the multislice approach to correct for the aberrations in the field in between the slices.

Further we note the similarity between the of blind deconvolution and the BPM model. This is mainly because of the scattering effect. Thus, each propagation and scattering operation can be

thought of as blurring of the input wave.

Following [12], we restate our problem.

$$\min_{n \geq 1, u} \mathcal{H}(n, u) := f_1(n) + f_2(u) + \|\mathcal{T}(n; u) - u_{meas}\|^2 + \kappa_1 \mathcal{R}_\varepsilon(n), \quad n \in \mathbb{R}_+^{N \times N \times N}, u \in \mathbb{R}^{2(N \times N)} \times \mathbb{R} \quad (4.2)$$

such that the initial incident plane wave $u(x, y, 0) = E_{in}$. Further, we take $f_1(n) \equiv 0$ and $f_2(u) \equiv 0$.

Next, there are two important properties that the objective function, $\mathcal{H}(n, u)$, must satisfy in order for the PALM method to be applicable; $\mathcal{H}(n, u)$ must be (partial) Lipschitz continuous and should satisfy the Kurdyka-Lojasiewicz (KL) property. We note the definition of these.

Proximal operator

We begin the section by introducing the *proximal operator*. Many gradient based optimization methods rely on the concept of projecting the gradient update onto a set which has certain desired properties based on the optimization problem. This set can be defined by a function, called the proximal operator.

Definition 4.2.1 (Proximal Operator) *The proximal operator of a convex function, $\sigma : X \rightarrow \mathbb{R}$, is defined as the map,*

$$prox_t^\sigma : X \rightarrow X, \quad prox_t^\sigma(w) = \arg \min_x \left\{ \sigma(x) + \frac{1}{2t} \|w - x\|^2 \right\} \quad (4.3)$$

where $t > 0$.

This operator can be seen as a generalization of the projection operator. Note that for $\sigma \equiv 0$ the $prox_t(n_p - \frac{\partial \mathcal{E}}{\partial n})$ we get our standard gradient descent method.

We follow [12] to define the KL property.

Kurdyka-Lojasiewicz(KL) property:

For $\eta \in (0, \infty]$ define the class of desingularizing functions as,

$$\Phi_\eta \equiv \left\{ \varphi \in C[[0, \eta), \mathbb{R}_+] \text{ such that } \begin{cases} \varphi(0) = 0 \\ \varphi \in C^1 & \text{on } (0, \eta) \\ \varphi'(s) > 0 & \forall s \in (0, \eta) \end{cases} \right. \quad (4.4)$$

A function g is said to satisfy the KL property at $\bar{u} \in \text{dom } \partial g$ if there exist $\eta \in (0, \infty]$, a neighborhood U of \bar{u} and a function $\varphi \in \Phi_\eta$, such that,

$$\forall u \in U \cap [g(\bar{u}) < g(u) < (g(\bar{u}) + \eta)]$$

the following holds

$$\varphi(g(u) - g(\bar{u})) \text{dist}(0, \partial g(u)) \geq 1 \quad (4.5)$$

where for any subset $S \subset \mathbb{R}^d$ and any point $x \in \mathbb{R}^d$

$$\text{dist}(x, S) := \inf\{\|x - y\| : y \in S\}$$

We assume that our objective function, eq.(2.11), satisfies the KL property.

Assumption A :

- i $f_1 : \mathbb{R}^{N \times N} \rightarrow (-\infty, \infty]$ and $f_2 : \mathbb{R}^{2(N \times N)} \rightarrow (-\infty, \infty]$ are proper and lower semi-continuous functions such that $\inf_{\mathbb{R}^{N \times N}} f_1 > -\infty$ and $\inf_{\mathbb{R}^{2(N \times N)}} f_2 > -\infty$
- ii Let $\mathcal{H}(n, u) = \|\mathcal{J}(n, u; E_{in}) - u_{meas}\|^2 + \alpha \mathcal{R}(n)$. Then, $\mathcal{H}(n, u)$ is differentiable and $\inf\{\mathcal{H}\} > -\infty$.
- iii For fixed u the function $n \mapsto \mathcal{H}(n, u)$ has its partial gradient to be Lipschitz continuous. That is,

$$\|\nabla_n \mathcal{H}(a, u) - \nabla_n \mathcal{H}(b, u)\| \leq K_1(u) \|a - b\|, \quad \forall a, b \in \mathbb{R}^{N \times N} \quad (4.6)$$

Similarly, for fixed n the function $u \mapsto \mathcal{H}(n, u)$ has its partial gradient to be Lipschitz continuous.

- iv For $j = 1, 2$ there exists $\sigma_j^-, \sigma_j^+ > 0$ such that

$$\inf\{K_1(u) : u \in B_2\} \geq \sigma_1^- \text{ and } \inf\{K_2(n) : n \in B_1\} \geq \sigma_2^- \quad (4.7)$$

$$\sup\{K_1(n) : u \in B_2\} \geq \sigma_1^+ \text{ and } \sup\{K_2(n) : n \in B_1\} \geq \sigma_2^+ \quad (4.8)$$

for any compact set $B_1 \subseteq \mathbb{R}^{N \times N}$ and $B_2 \subseteq \mathbb{R}^{2(N \times N)}$.

- v $\nabla \mathcal{H}$ is Lipschitz continuous on bounded subsets of $\Omega_1 \times \Omega_2$. ($\Omega_1 \subset \mathbb{R}^{(N \times N)}$, $\Omega_2 \subset \mathbb{R}^{2(N \times N)}$)

We further assume that the objective function satisfies the above assumptions. Now we calculate the partial Lipschitz constant with respect to the field.

Let u_{in} the incident plane wave and u_m be the field after scattering through the m^{th} slice,

$$\begin{aligned}\nabla_{u_m} \mathcal{H} &= \nabla_{u_m} \|\mathcal{T}(n, u_{in}) - u_{meas}\|^2 \\ &= \nabla_{u_m} \|\mathcal{C}_M u_{in} - u_{meas}\|^2 \\ &= \nabla_{u_m} \|\mathcal{A}_{m+1} u_m - u_{meas}\|^2 \\ &= \mathcal{A}_{m+1}^\dagger (\mathcal{A}_{m+1} u_m - u_{meas})\end{aligned}$$

where we used the derivative as in Wirtinger calculus, [13]. Let $u_{in}^{(1)}$ and $u_{in}^{(2)}$ be two incident wave which have only a small phase difference and, $u_m^{(1)}$ and $u_m^{(2)}$ be the two wave after scattering through the m^{th} slice, then we can assume that measured complex fields are quite close. Let the difference be $u_{meas}^{(2)} - u_{meas}^{(1)} = \delta$. Then we have,

$$\begin{aligned}\left\| \nabla_{u_m^{(1)}} \mathcal{H} - \nabla_{u_m^{(2)}} \mathcal{H} \right\| &= \left\| \mathcal{A}_{m+1}^\dagger (\mathcal{A}_{m+1} u_m^{(1)} - \mathcal{A}_{m+1} u_m^{(2)} + \delta) \right\| \\ &\leq \left\| \mathcal{A}_{m+1}^\dagger (\mathcal{A}_{m+1} u_m^{(1)} - \mathcal{A}_{m+1} u_m^{(2)}) \right\| + \left\| \mathcal{A}_{m+1}^\dagger \delta \right\|\end{aligned}$$

Since $\|\cdot\|_2$ is unitary invariant and the operator norm of an unitary operator is 1 we have,

$$\left\| \nabla_{u_m^{(1)}} \mathcal{H} - \nabla_{u_m^{(2)}} \mathcal{H} \right\| \leq c \left\| u_m^{(2)} - u_m^{(1)} \right\| \quad (4.9)$$

where $c > 1$. Since u lies in the complex field, we can assume it to be in the 2D real space (since \mathbb{C} and \mathbb{R}^2 are isomorphic). Thus, the gradient is equivalent to taking the gradient with respect its components (real and imaginary). We explicitly calculated the gradient w.r.t the refractive index in Chapter 2 along with its Lipschitz constant. And it is easy to see that the other assumptions are satisfied as well.

We now state the PALM algorithm

Algorithm 4 Proximal Alternating Linearized Minimization

- 1: **procedure** PALM
 - 2: Initialize $n = n_0$, $u = u_{in}$, tolerancelevel = tol
 - 3: **while** error > tol **do**
 - 4: $t = t + 1$
 - 5: **for** j=1 : J **do**
 - 6: **for** m=1:M **do**
 - 7: Choose $\gamma_1 > 1$, $\tau_t = \gamma_1 K_1(u_j^t)$
 - 8: $n_m^{t+1} \in \text{prox}_{\tau_t}^{f_1} \left\{ n_m^t - \frac{1}{\tau_t} \frac{\partial \mathcal{H}(z_1^t, u^t)}{\partial n} \right\}$
 - 9: Choose $\gamma_2 > 1$, $\omega_1 = \gamma_2 K_2(n_m^{t+1})$
 - 10: $u_j^{t+1} \in \text{prox}_{\omega_1}^{f_2} \left\{ u_j^t - \frac{1}{\omega_1} \frac{\partial \mathcal{H}(n_m^{t+1}, u_j^t)}{\partial u} \right\}$
 - 11: Calculate Error between measured and computed field.
 - 12: **return** n and error
-

The algorithm basically does two things; update the refractive index and correct the field. To update the refractive index we calculate the gradient as we did in Chapter 2. And now to update the field as we do as follows; since the incident wave is a plane wave, it can be represented by a single point in the frequency plane. See figure . As this plane wave passes through a sample with varying refractive index, one can see the amount of scattering that occurs by looking at the scattered wave in the frequency plane. We write the update steps 8 as follows,

$$n_m^{t+1} = n_m^t - \frac{1}{\tau_t} \frac{\partial \mathcal{H}(z_1^t, u^t)}{\partial n_m}$$

for the refractive index of the m^{th} slice. Then, step 10 is given by,

$$y = \mathcal{F}(u_j^t) - \mathcal{F}\left(\frac{1}{\omega_t} \frac{\partial \mathcal{H}(n_m^{t+1}, u_j^t)}{\partial u_j}\right)$$

$$u_j^{t+1} = \mathcal{F}^{-1}(y)$$

for the j^{th} observation after scattering through the m^{th} slice.

4.3 Remarks

We would like to highlight the resemblance between the PALM method and the non-convex approach. The PALM method is based on two elements; by breaking the problem into blocks and using proximal steps to make the updates. While, the non-convex approach was introduced on the basis of the nature of minimization. But, the non-convex approach can be seen in the PALM formulation as follows. Every set of two consecutive slices in the BPM model which represent the refractive index distribution, can be considered to be two blocks. These two blocks are updated such that the update for the second block depends on the update for the first block. This is basically the PALM method.

Chapter 5

Results and Discussion

We start this chapter by describing the phantom data and its details. Then, we present the main results of this study. With the given results we analyze them by addressing our research questions. Finally, we draw conclusions based on the analysis.

Phantom Data and Parameters

In all our simulations we use phantom data created in MATLAB. The phantom data represents a collection of small beads of diameter 4-20 μm . These beads are supposed to represent biological cell suspended in a medium of refractive index of 1.36. So the background index is about 1.36. The beads themselves have two parts; a core and a shell (refractive index 1.385-1.41). The choice of the refractive index in the range 1.385-1.41 is motivated from [14]. Next, we use plane waves of wavelength 0.6328 μm . We take 64 observations with angles in the z-direction ranging from -45° to 45° and $0^\circ - 360^\circ$ in the xy-plane. The thickness of the sample is chosen from 30 μm to 85 μm . Further, the spacing between the slices, that is the size of discretization of the sample, is 0.20 μm . In all our simulations we use the TV regularization with $\alpha = 0.0003$.

5.1 Research Goals

Recalling our research goals, from Section 1.2, we address the following questions:

Q1 : What is the relation between thickness of the sample and the quality of reconstruction?

Q2 : Which optimization model shows promise for the best reconstruction?

First, we need a systematic way to address Q1. There are two approaches through which we can analyze the relationship between sample thickness and the quality of reconstruction. In both the method we use the *residual* between the original phantom and the reconstructions. In the following section we describe a metric to assess the quality of the reconstruction.

Residual

Our phantom data and the reconstructions are 3D dimensional data sets. Then, the residual for such a data set can be defined as follows; let $n_{original}$ be the original phantom data and the n_{recon} be the reconstructed data. The residual between $n_{original}$ and n_{recon} can be defined as

$$r_{res} = \frac{\sum |n_{original} - n_{recon}|}{M \times L \times L}$$

where the sum is taken over all the elements of the 3D array. M represents the number of slices and the $L \times L$ represents the number of pixels for each slice.

As mentioned there are two ways we use the residual to analyze the quality of the reconstruction:

A1 : Residual of the refractive index distribution vs. increasing the thickness of the sample.

A2 : Residual of the refractive index distribution vs. the optimization method for different thickness.

We explore the above two methods in Section 5.2. In the following section we show some typical results of our reconstructions.

Sample Reconstruction

In the following figure we show the reconstruction of a $50 \mu\text{m}$ thick phantom sample containing small beads of $5\text{-}10 \mu\text{m}$ in diameter. The refractive index of the beads and the medium can be seen in the values corresponding to the scale values. The pixel size is 256×256 and the dimensions of the cross section of the sample are $100\mu\text{m} \times 100\mu\text{m}$. The iterations were stopped at 40.

Figure 5.1(a) shows the original phantom data, while Figures 5.1(b)-(d) show the reconstructions. In Figure 5.1(b) it is interesting to see that using the standard gradient descent method, where one takes the average of all the observations, the diffraction artifacts add up to produce a blurred image.

Figure 5.1(c) shows the reconstruction result by the non-convex approach. Compared to the Gradient descent, the non-convex approach produces a far better reconstruction in terms of the structure. Especially, the reconstruction around the edges is quite accurate. In terms of the refractive index values, the approach has less effect in the background. Moreover, due to the padded boundaries one can notice the diffraction artifacts caused by the edges. But since we know that the background is smooth and have sharp boundaries for the beads, by applying the TV regularizer, we have an improvement in the reconstruction for the background as well as the refractive index values.

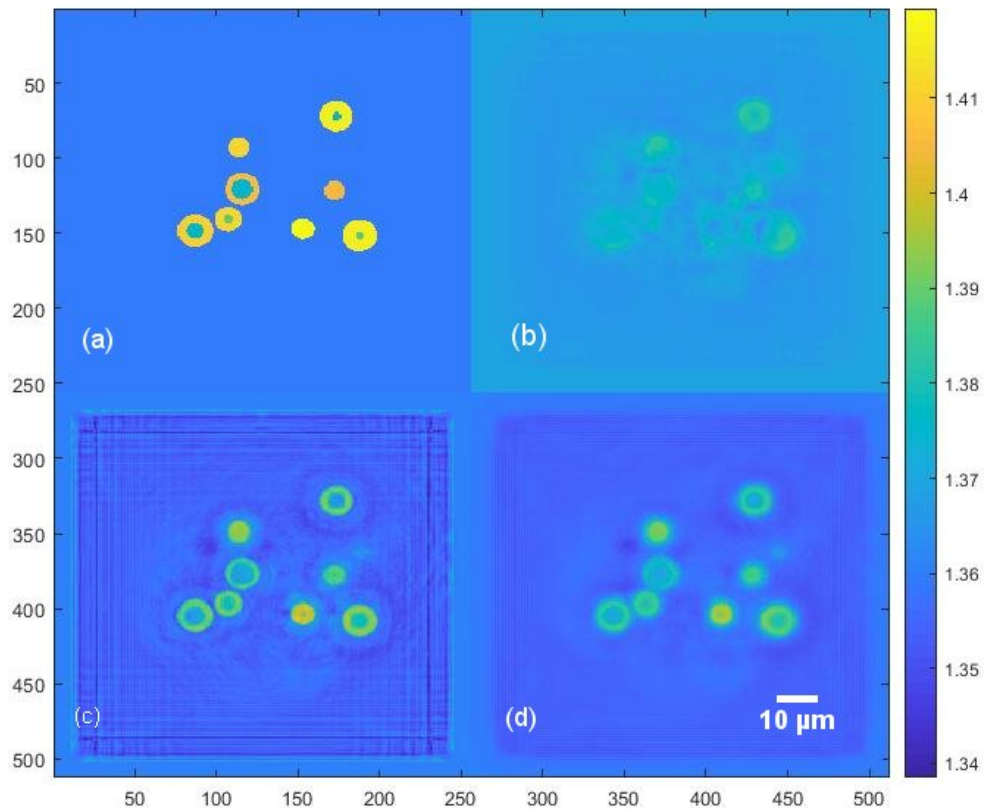


Figure 5.1 Images of original and reconstructed slices. The scale in the x-y directions show pixels. The size of each reconstruction is $50 \mu\text{m} \times 50 \mu\text{m}$. (a) Original Phantom. (b) Reconstruction using Gradient descent: $r_{res} = 2.7 \times 10^{-3}$. (c) Reconstruction using non-convex approach. (d) Reconstruction using non-convex approach and TV regularizer: $r_{res} = 1.3 \times 10^{-3}$.

5.2 Analysis

In this section the main goal is to address the quality of reconstruction, which is done in two ways, A1 and A2. To have a fair comparison we began all the reconstruction with same settings, that is, same initial conditions and parameters. We also note that for a given sample to achieve a reconstruction of optimal quality one needs to adjust the parameters and have good initial guess. In our comparison we only take one data set for each thickness. This is mainly due to the computational time required for the reconstructions. For a more accurate representation of the results one would require averaging over many different structures. To begin with, we see the convergence behavior of the non-convex approach and the Gradient descent.

5.2.1 Convergence Behavior

The following plot show the convergence and the difference between consecutive updates for a $50 \mu\text{m}$ thick sample. The iterations are stopped at 15 iterations because the non-convex method becomes parallel to x-axis.

The quality of reconstruction gives an idea about how well the reconstruction algorithms perform. But, it is also necessary to see the convergence of total energy of the objective function. Figure 5.2 shows the energy w.r.t the number of iterations. The non-convex method's energy quickly drops in about 7 iterations, while the gradient is quite slow in terms of convergence. Apart from the decrease in energy it is also fruitful to see the difference between consecutive updates. This difference in consecutive updates would reflect gradient value. One would expect that at a critical point the gradient is zero. Therefore, if the difference in the updates goes to zero, it suggests that the algorithm is near a critical point.

From the Figure 5.3 one can see that the non-convex method has decreasing difference in updates with the increase in number of iterations. Whereas, Gradient descent has almost no change in the difference in the updates. This suggests that the non-convex method reaches a critical point quickly as compared to the Gradient descent. This is an important point to note, since in the next section we will discuss the sensitivity of the method to initial conditions, where the a good initial conditions is required for the minimization problem to reach an optimum.

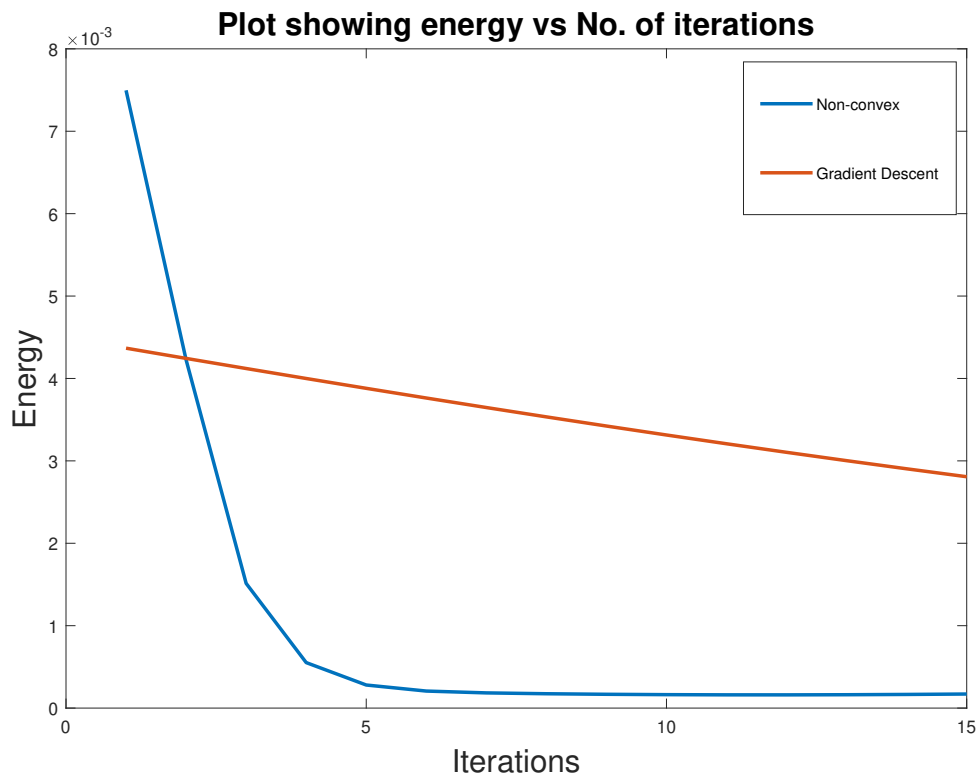


Figure 5.2 Plot showing the drop in energy of the objective functions for non-convex approach (with TV regularizer) and Gradient Descent method.

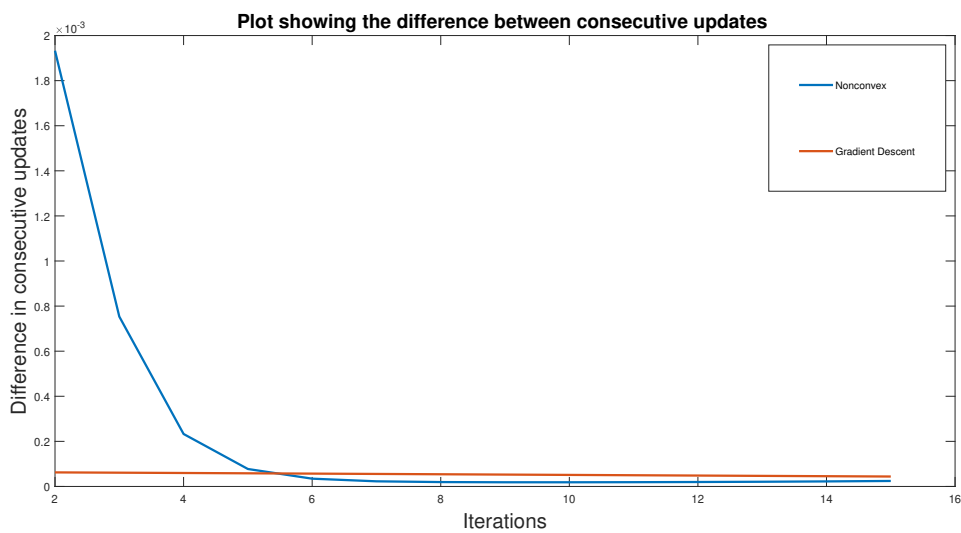


Figure 5.3 Plot showing difference between consecutive updates after each iteration for non-convex approach and Gradient Descent method.

5.2.2 Residual Comparison

Before we proceed, it is important to mention few notes about the sample points plotted in the Figure 5.5. The reconstruction obtained through the non-convex approach results in some frames being inverted. This is because of the non-convexity of the problem. To analyze this non-convex behavior we look at the reconstructions with different initialization, i.e. with a different guess for the refractive index map.

Sensitivity to initial conditions

Figure shows the result of reconstruction with different initialization. Here, it is quite interesting to see that when periodic boundary conditions are applied the non-convex behavior is clearly visible. While, the results in the previous section, where padded boundaries were applied, the resulting solution was clearly better. But, with the padded boundaries induced lot of diffraction artifacts. The BPM model requires the refractive index distribution for the simulation of light propagation. The iterative procedure of reconstruction relies on the assumption that, at every step you get closer to the correct value by updating the refractive index values. So, given a set of measurements one must have good initial guess of the refractive index of the medium to begin with. Figure 5.4 shows the reconstruction of a $50 \mu\text{m}$ thick sample with different initial guess for the background after a few iterations. In the reconstructions Figure 5.4(a) and 5.4(d) , the reconstructions is not correct since the direction of the update is wrong. While in Figure 5.4(c), the reconstruction is accurate in terms of the structure and the direction of the updates. We also see some artifacts because of the limitation of number of observations one can take.

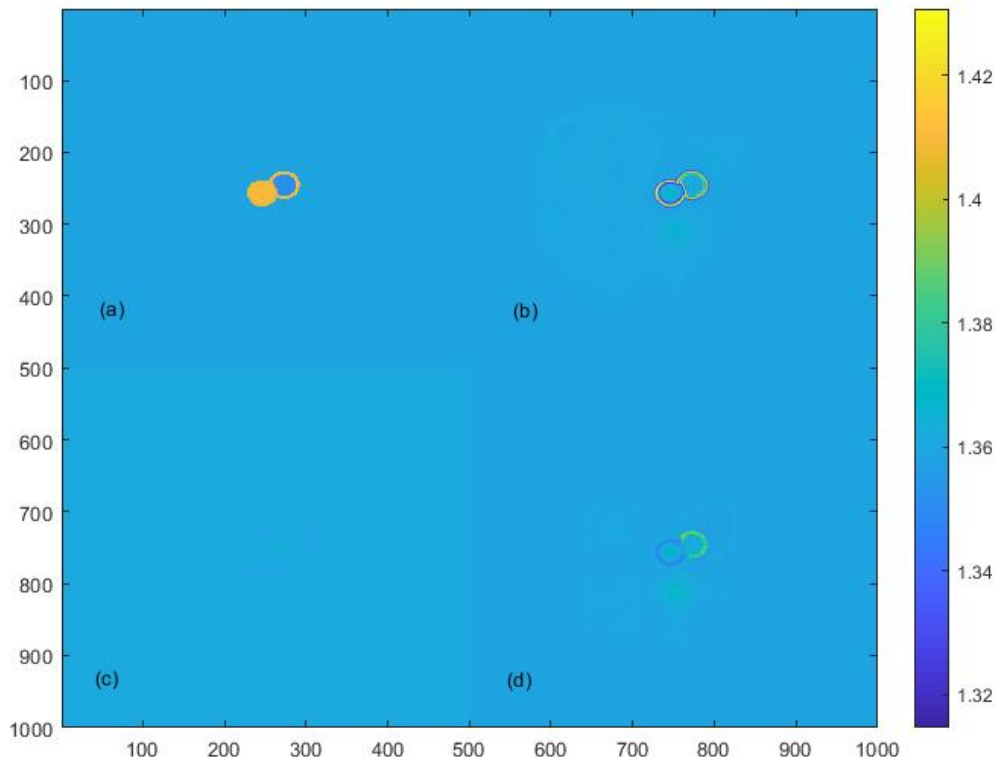
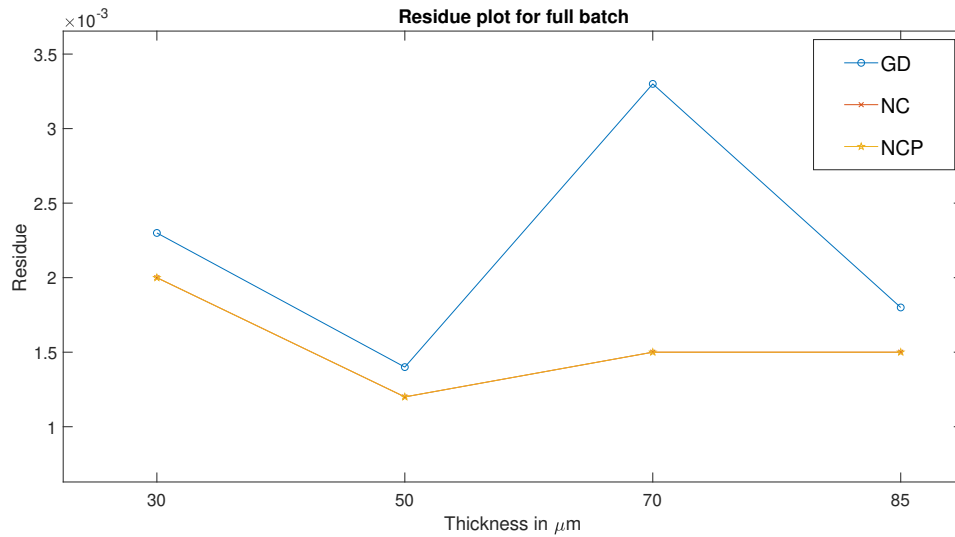


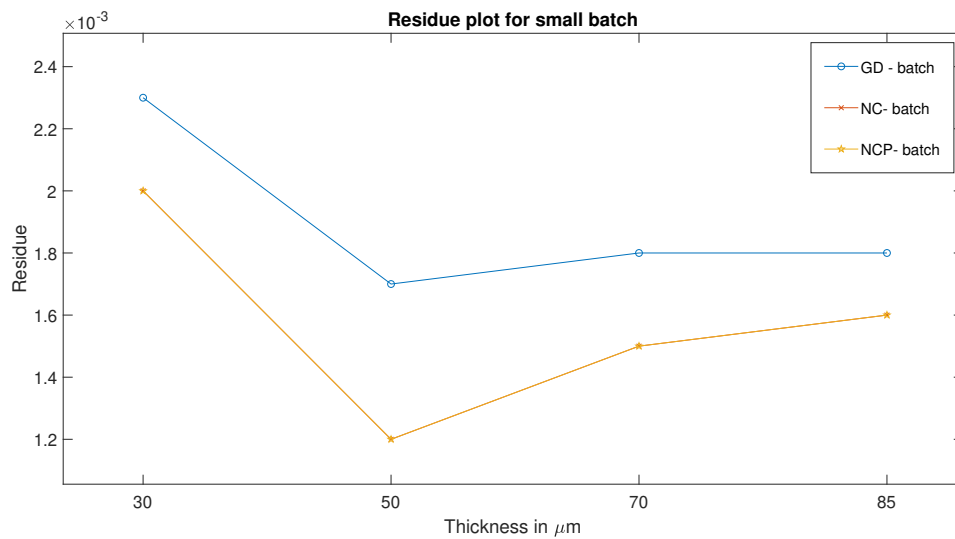
Figure 5.4 Reconstruction of a $50\mu\text{m}$ thick sample with different initialization of the background. The size of the sample is $230\mu\text{m}\times 230\mu\text{m}$ (500 pixels) in the x-y plane. The axis show number of pixels. (a) Original. (b) non-convex with initialization at 1.365. (c) Gradient descent with initialization at 1.365. (d) non-convex with initialization at 1.36

Residual vs. Sample Thickness

Figure 5.5 shows the graphs of residue between the original phantom and the reconstructions. The first graph 5.5a shows the when one takes all the observation into account in every iteration, called full batch. In the following we note the observation from the graphs.



(a) Full batch



(b) Stochastic batch

Figure 5.5 Graph showing the residuals for different optimization methods with increasing thickness.

Residual vs Optimization method

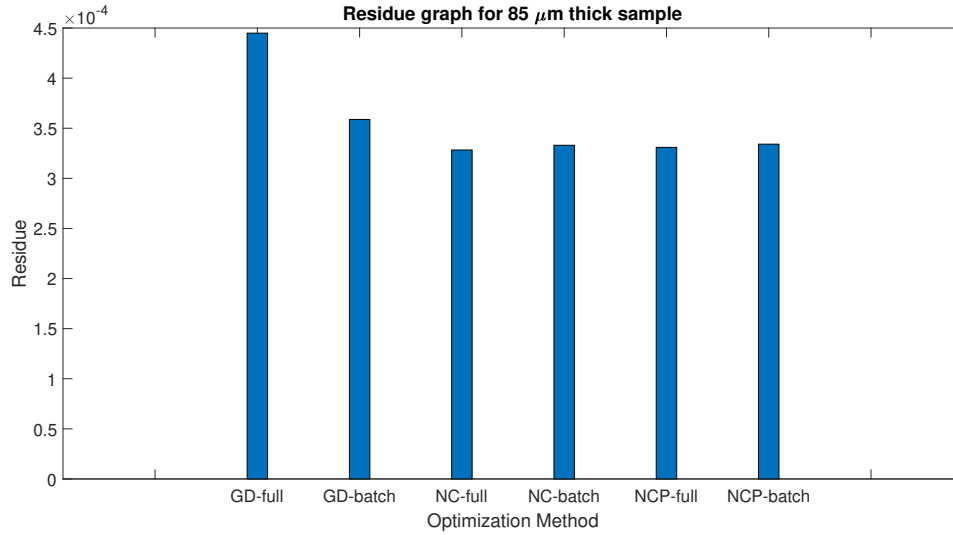


Figure 5.6

Graph showing the residual between the reconstructions and the original phantoms for different optimization methods

In the graph, from Figure 5.6, we see that the residue for Gradient descent has the highest value. And for the non-convex approach it is approximately 20% lower. This is also evident from the reconstruction result, Figure 5.1. Further, by tuning the parameters we expect that it is possible to achieve a lower residual.

Observations:

1. In Figure 5.5a, there is a drop in the residue from 70 μm to 85 μm . This is could be due to the initial conditions and parameters settings as mentioned earlier. The non-convex optimization has a lower residue for all the corresponding thickness.
2. In Figure 5.5b, we observe that the residues increases with increasing sample thickness.
3. There is almost no difference between the non-convex approach and non-convex with phase correction. This is could be because of small step size of the phase correction term, which results in having no visible change. Moreover, the if the step size is kept at zero the method is same as the non-convex approach

Interpretation:

1. The quality of the reconstructions seems to decrease as the sample thickness increases.

2. A solution for a better reconstruction could be by adapting both convex and non-convex method. Here, one can begin the reconstruction with the Gradient descent and then use the initial step as an initialization for the non-convex method.
3. Another solution could be by using clipping, that is, with some knowledge of the refractive index one could restrict the refractive index to be contained in bracket.

Chapter 6

Conclusion

In this study we used the Beam Propagation Model to simulate light propagation through a given refractive index distributions. Using this model we derived and implemented an algorithm for reconstructing refractive index distributions from the measured complex field, obtained by shining light through the sample.

We started this thesis by introducing the necessary motivation for studying the problem of reconstructing the refractive index distribution and why we use the BPM model to solve it. We also note that in practice one uses diffraction tomography based on the Born or the Rytov approximation. Then, we discussed the necessary elements of the BPM model which was required for modeling the inverse problem. It was mainly important in calculating the gradient, which was the main tool in all of our reconstruction methods.

We introduced two methods for reconstructions; Convex Optimization and Non-convex Optimization method. The Convex Optimization method was based on assumption that the objective function that is being optimized is a convex one. But, as we saw in the results section the Convex algorithm produces a blurred image. Whereas, by using the non-convex approach for formulating and optimizing the functional, we achieved a better reconstruction.

Finally, in Chapter 5, we answered our research questions; the relationship between quality of reconstruction and the sample thickness. To quantify the quality we introduced a metric, which is the residual between the original phantom and the reconstruction. We saw that the quality of reconstruction gets worse with increase in sample thickness. Further, we noted that in some slices of the reconstruction the refractive index was inverted. This was because of the non-convex nature of the problem. Then, we noted the importance of initial guess which is a crucial factor in the non-convex optimization method and proposed a solution which could be useful in a better reconstruction.

There are quite a few things that can be improved. By increasing the number of observations one can improve the quality of reconstruction. To better establish the relationship between the sample thickness and the reconstruction, averaging over more sample could be helpful. One can combine the reconstruction algorithms studied in this thesis with wavefront shaping to achieve a faster and a better reconstruction. By doing so one achieve many applications involving focusing of light and imaging through the sample.

Bibliography

- [1] I. M. Vellekoop, A. Lagendijk, and A. P. Mosk. Exploiting disorder for perfect focusing. *Nature Photonics*, 4:320 EP –, Feb 2010.
- [2] I. M. Vellekoop and A. P. Mosk. Focusing coherent light through opaque strongly scattering media. *Opt. Lett.*, 32(16):2309–2311, Aug 2007.
- [3] Paul Müller, Mirjam Schürmann, and Jochen Guck. The Theory of Diffraction Tomography. *arXiv e-prints*, page arXiv:1507.00466, Jul 2015.
- [4] Ulugbek S. Kamilov, Ioannis N. Papadopoulos, Morteza H. Shoreh, Alexandre Goy, Cedric Vonesch, Michael Unser, and Demetri Psaltis. Learning approach to optical tomography. *Optica*, 2(6):517–522, Jun 2015.
- [5] Jérôme Bolte, Shoham Sabach, and Marc Teboulle. Proximal alternating linearized minimization for nonconvex and nonsmooth problems. *Mathematical Programming*, 146(1):459–494, Aug 2014.
- [6] J. Van Roey, J. van der Donk, and P. E. Lagasse. Beam-propagation method: analysis and assessment. *J. Opt. Soc. Am.*, 71(7):803–810, Jul 1981.
- [7] Bernd Hofmann and Stefan Kindermann. On the degree of ill-posedness for linear problems with noncompact operators. *Methods and Applications of Analysis*, 17, 04 2011.
- [8] Ryan Tibshirani. Convex optimization lectures 2013. 2013.
- [9] B.T. Polyak. Some methods of speeding up the convergence of iteration methods. *USSR Computational Mathematics and Mathematical Physics*, 4(5):1 – 17, 1964.
- [10] Lei Tian and Laura Waller. 3d intensity and phase imaging from light field measurements in an led array microscope. *Optica*, 2(2):104–111, Feb 2015.
- [11] A. M. Maiden, M. J. Humphry, and J. M. Rodenburg. Ptychographic transmission microscopy in three dimensions using a multi-slice approach. *J. Opt. Soc. Am. A*, 29(8):1606–1614, Aug 2012.
- [12] Thomas Pock and Shoham Sabach. Inertial Proximal Alternating Linearized Minimization (iPALM) for Nonconvex and Nonsmooth Problems. *arXiv e-prints*, page arXiv:1702.02505, Feb 2017.
- [13] Raphael Hunger. An introduction to complex differentials and complex differentiability. *TUM-LNS-TR-07-06*, 2007.
- [14] Willem F. Decraemer Joris J. Dirckx, Liesbeth C. Kuypers. Refractive index of tissue measured with confocal microscopy. *Journal of Biomedical Optics*, 10(4):1 – 8 – 8, 2005.

Appendix A

Definition A.0.1 (Convex/Concave) Let C be a convex set, such that $C \subseteq X$ where X is vector space. A function $f : C \rightarrow \mathbb{R}$ is called convex on C if,

$$f(\lambda x + (1 - \lambda)y) \leq \lambda f(x) + (1 - \lambda)f(y)$$

for all $x, y \in C$ and $0 \leq \lambda \leq 1$.

If $-f$ is convex, then f is concave.

Definition A.0.2 (Linear Map) Let V, W be two vector spaces of finite dimension. For $L : V \rightarrow W$, L is called linear if $\forall v_1, v_2 \in V$ we have,

$$L(av_1 + bv_2) = aL(v_1) + bL(v_2)$$

Definition A.0.3 (Fourier Transform) Let $f : X \rightarrow \mathbb{C}$ such that $f \in L_2$. Then the Fourier transform of f , denoted $\mathcal{F}(f) = \hat{f}$, is given by,

$$\mathcal{F}(f(x)) = \hat{f}(\eta) = \int_{-\infty}^{\infty} f(x)e^{-i\eta x} dx$$

We will usually deal with 2D-Fourier transform where the transform is taken in 2 dimensions and the exponent, $e^{i\eta x}$, is replaced by the dot product, $e^{i\eta \cdot x}$.

Definition A.0.4 (Subderivative) Let V be real vector space. The subderivative of a convex functional, $f : V \rightarrow \mathbb{R}$, at a point $x_0 \in V$ is the vector w such that,

$$f(x) \geq f(x_0) + \langle w, x - x_0 \rangle \tag{A.1}$$

Definition A.0.5 (Subdifferential) The set of all subderivatives of a convex functional, f as defined above, is called the subdifferential of the function f , denoted by ∂f .

Figure 1.1 link : https://upload.wikimedia.org/wikipedia/commons/thumb/3/3f/Refraction_at_interface.svg/669px-Refraction_at_interface.svg.png.